Supplementary Material for

A central neural circuit for itch sensation

Di Mu, Juan Deng, Ke-Fei Liu, Zhen-Yu Wu, Yu-Feng Shi, Wei-Min Guo, Qun-Quan Mao, Xing-Jun Liu, Hui Li, Yan-Gang Sun*

*Corresponding author. E-mail: yangang.sun@ion.ac.cn.

This PDF file includes:

Materials and Methods
Figs. S1 to S14
References

Other Supplementary Material for this manuscript includes the following:
(available at www.sciencemag.org/content/357/6352/695/suppl/DC1)

Movie S1

Materials and Methods

Animals

Male C57BL/6N, $Vglut2^{f/f}$, $Vglut2\text{-}Cre$, gastrin-releasing peptide receptor-iCreERT2 (GRPR-iCreERT2) mice were used for experiments. C57BL/6N was purchased from SLAC laboratory (Shanghai). $Vglut2^{f/f}$ mice (JAX 012898) and $Vglut2\text{-}Cre$ (JAX 016963) were initially acquired from the Jackson laboratory. GRPR-iCreERT2 mice were made by Beijing Biocytogen by inserting the 2A-linked optimized Cre recombinase fused with the ligand-binding domain of the estrogen receptor (2A-iCreERT2) cassette in the 3'UTR of $Grpr$ gene in order to mimic the endogenous expression of GRPR. All mice were raised on a 12-hr light/dark cycle (lights on at 7:00 am) with $ad libitum$ food and water. All behavioral tests were carried out during the light phase. All procedures were approved by the Animal Care and Use Committee of the Institute of Neuroscience, Chinese Academy of Sciences, Shanghai, China.

Stereotaxic injection

To manipulate the activity of PBN neurons, adeno-associated viruses (AAV) were injected into the PBN of 2- to 3-month-old mice and behavioral tests were performed 4-6 weeks after viral injection. For slice recording, 2-6 week-old mice were used for viral injection, and recording was performed 2-6 weeks after the viral injection. All stereotaxic injection were performed with a stereotaxic apparatus, and body temperature of the animal was maintained with a heating pad. Ophthalmic ointment was applied to maintain eye lubrication. Viruses or retrobeads were injected at a rate of ~50 nl/min using an air pressure system by connecting to glass pipettes (tip diameter of 10-30 μm). After the injection, the glass pipettes were left in place for 5-10 min before withdrawal to allow for diffusion. The animals were allowed to recover from anesthesia on a heating blanket before returning to their home cage. Antibiotics (Ceftriaxone sodium, 0.1 g/kg) was injected intraperitoneally for three days after surgery to prevent infection.

Surgery for injection into the PBN

Mice were anesthetized with pentobarbital sodium (0.1 g/kg) and mounted in a stereotaxic apparatus. The skull was exposed by midline scalp incision, and craniotomy was performed unilaterally or bilaterally for introduction of a microinjection glass pipette into the PBN (5.20 mm posterior to bregma, ±1.25 mm lateral to midline, 3.5 mm ventral to skull surface). The craniotomy window (~1.5 mm diameter) was made using a hand-held drill over the target area. For deleting $Vglut2$ in the PBN, $Vglut2^{f/f}$ mice were bilaterally injected with an AAV expressing Cre-EGFP (AAV-hSyn-Cre-EGFP, AAV2/8, titer: 8.7×10^{12} v.g./ml) at a volume of 400 nl for each side, or AAV-hSyn-EGFP virus (AAV2/8, titer: 3.6×10^{12} v.g./ml) for the same volume as control. For manipulating the neuronal activity of the PBN with DREADDs, AAV-hSyn-HA-hM4Di-IRES-mCitrine virus (AAV2/9, titer: 1.0×10^{13}

v.g./ml) was injected bilaterally at a volume of 150 nl for each side, and AAV-hSyn-EGFP virus (AAV2/8, titer: 3.6×10^{12} v.g./ml) was used as control.

In order to examine the efficacy of blocking glutamatergic synaptic output of the PBN after genetic deletion of *Vglut2*, *Vglut2^{f/f}* or wild-type mice were injected with 600~800 nl of mixture of AAV-hSyn-Cre-EGFP (AAV2/8, titer: 4.4×10^{12} v.g./ml) and AAV-Ef1α-DIO-ChR2(H134R)-mCherry (AAV2/8, titer: 2.0×10^{12} v.g./ml) into the PBN (right side). The animals were used for slice electrophysiology recording 5-6 weeks after viral injection.

In order to monitor the neuronal activity of PBN neurons during pruritogens-induced scratching behavior, C57BL/6N mice were injected with 300 nl of AAV-hSyn-GCaMP6s virus (AAV2/9, titer: 5.3×10^{12} v.g./ml) or AAV-hSyn-EGFP virus (AAV2/8, titer: 4.4×10^{12} v.g./ml) as control into the left PBN (5.20 mm posterior to bregma, 1.25 mm left to midline, 3.5 mm ventral to skull surface). *Vglut2-Cre* mice were injected with 300 nl of AAV-hSyn-DIO-GCaMP6s (AAV2/9, 2.8×10^{12} v.g./ml) virus or AAV-Ef1α-DIO-EYFP virus (AAV2/9, 5.5×10^{12} v.g./ml) as control into the left PBN.

For behavioral experiments, animals were allowed to recover for 3 weeks. The mice were then handled and habituated with the behavioral environment every day for one week. For surgery followed by spinal c-Fos immunostaining, red fluorescent retrobeads (400-600 nl) were injected into left PBN and histamine was injected into right side of the nape. For surgery followed by slice electrophysiology recording, red fluorescent retrobeads (400-600 nl) were injected into bilateral PBN. Animals were used for immunohistochemistry or spinal cord slice recording 3-5 days after the retrobeads injection. For all experiments, the animals with incorrect injection sites were excluded from further analysis.

Surgery for intra-spinal cord injection

For spinal injection of the AAV virus, mice were anesthetized with 0.2 g/kg ketamine and 0.01g/kg xylazine. Cervical vertebrae were exposed at C4-C6, and the vertebral column was mounted in a stereotaxic frame. Laminectomy was performed, and the dura was incised to expose the spinal cord. AAV-EF1α-DIO-ChR2(H134R)-EYFP (AAV2/9, titer: 5.1×10^{12} v.g./ml), AAV-EF1α-DIO-EYFP (AAV2/8, titer: 4.4×10^{12} v.g./ml), AAV-hSyn-ChR2(H134R)-mCherry (AAV2/8, titer: 4.0×10^{12} v.g./ml), AAV-hSyn-eNpHR3.0-EYFP (AAV2/9, titer: 1.7×10^{13} v.g./ml), or AAV-hSyn-EGFP (AAV2/8, titer: 4.4×10^{12} v.g./ml) were injected into the right side of the spinal cord at 2-4 injection sites (interspaced by 400 μm, 400-600 nl of AAV was injected for each site). Micropipette was inserted into the dorsal spinal cord at an angle (50-60 degrees) to target at the superficial dorsal horn. The micropipette was withdrawn 5 min after viral injection. Incision was closed with stitches.

Tamoxifen injection

Tamoxifen was dissolved at 20 mg/ml in sunflower oil by vibration for 2-4 hours at room temperature. GRPR-iCreERT2 mice used for spinal slice recording or fiber

photometry were intraperitoneally (i.p.) injected with tamoxifen (150 mg/kg) daily for three successive days. GRPR-iCreERT2 mice used for immunostaining were injected with tamoxifen (150 mg/kg, i.p.) daily for five successive days.

Implantation of optical fibers in the PBN

For optogenetic suppression of the spinoparabrachial pathway, the animals were implanted with optical fibers (NA 0.37) targeting at the bilateral PBN (5.2 mm posterior to bregma, ±1.9 mm lateral to midline, 2.7 mm ventral to skull surface) at an angle (15 degrees) two weeks after the injection of AAV-hSyn-eNpHR3.0-EYFP or AAV-hSyn-EGFP in the spinal cord. Optical fibers were attached to the skull with dental cement.

For monitoring the activity of PBN neurons with fiber photometry, optical fibers (NA 0.37) were implanted to target the left PBN (5.2 mm posterior to bregma, 1.25 mm lateral to midline, 3.5 mm ventral to skull surface) one week after injection of AAV in the PBN.

Itch behavioral test

For automatic assessment of scratching behavior, a magnet (1 mm in diameter, 3 mm in length) was implanted into the back of right hindpaw for each mouse under anesthesia (pentobarbital sodium, 0.1 g/kg) at least 7 days before the behavioral tests (*31*). Ceftriaxone sodium (0.1g/kg) was intraperitoneally injected to prevent infection. Mice were shaved on the right back of the neck and individually handled daily for 5 days before the behavioral tests. Mice were injected with saline intradermally or intrathecally, then habituated with the recording chamber for 30 min during the last three days. During behavioral experiments, baseline was recorded with a magnetic induction method for 15 min in a cylinder chamber (20-cm high, 15-cm in diameter) surrounded by a coil. Then, the mice were briefly removed from the chamber and intradermally injected with pruritic compounds, histamine (500 μg/50 μl), chloroquine (200 μg/50 μl), compound 48/80 (100 μg/50 μl) or endothelin-1 (25 ng/50 μl), 5-HT (10 μg/50 μl), HTMT (0.1 μmol/50 μl), Clobenpropit (0.1 μmol/50 μl) into right side of the nape. Bombesin (0.2 nmol/10 μl) was intrathecally injected. For bombesin, only the scratching behavior of the right hindpaw was analyzed, even the animal scratch with both hindpaws. Scratching behavior was recorded for 30-90 min after injection with the magnetic induction method, using a customized recording system following the established method (*31*). The scratching behavior was analyzed with custom-written codes in Matlab.

In some experiments, the scratching behavior was videotaped with a high speed camera (120 Hz), and was recorded with the magnetic induction method simultaneously. The scratching behavior was analyzed manually to compare with the results obtained with the magnetic induction method.

Allergic itch

In the allergy model of itch (*32*), ovalbumin (50 μg) and Imject™ Alum Adjuvant (2 mg) were dissolved in 250 μl of phosphate-buffered saline (PBS) and

intraperitoneally injected for the first sensitization. Same treatment was carried out 10 days later for the second sensitization. One week later, ovalbumin (50 μg/50 μl) was injected intradermally to right side of nape, and the scratching behavior was recorded for 30 min.

Chronic itch

Mice were painted with 100 μl of 1-Fluoro-2,4-dinitrobenzene (DNFB) acetone solution (0.1%) onto the shaved abdominal skin for initial sensitization. Cutaneous reaction was evoked in the right clipped back part of sensitized mouse neck by repeated paintings with 50 μl of DNFB acetone solution (0.1%). The DNFB challenge was repeated twice a week for 4 weeks, 9 times in total, starting from 7 days after the initial sensitization. Scratching behavior was recorded 1 hr or 24 hr after DNFB painting.

Nociceptive behavior

Animals were habituated to the behavioral room for at least two days before behavioral tests. The behavioral tests were performed as described previously (*33*). For testing mechanical sensitivity, mouse hindpaw was perpendicularly stimulated with a series of von Frey hairs with logarithmically incrementing stiffness (0.16-2.56 grams). The 50% paw withdrawal threshold was determined using up-down method (*34*).

For examining thermal pain, the paw withdrawal latency to a noxious thermal stimulus was determined as the average of at least four measurements per paw over a 5-min test period using Hargreaves apparatus, and a 20-sec cutoff time was set to avoid tissue damage.

For the tail immersion test, mice were gently restrained with a cotton thread glove. The protruding one-third of the tail was then dipped into a water bath of 50 ℃. And the tail flick latency was recorded, with a cutoff time of 10 seconds to avoid tissue damage.

Open field test

Locomotor activity of mice was evaluated by open-field test over a 10-min (or 15-min) period in (40 × 40 × 40 cm) polystyrene enclosures as described previously (*35*). Mice were placed in the center of the box and were videotaped individually. Center area is defined as centric 20 x 20 cm. The track was analyzed by LabState. Total distance traveled (in cm) and time spent in the center area was analyzed. To examine the effect of optogenetic suppression of spinoparabrachial pathway on mouse locomotive activity, mice were tested for a 15-min session (consisting of 5-min light OFF, 5-min light ON, and 5-min light OFF periods). Constant laser (593 nm, 8-10 mW) was delivered bilaterally during the light ON phase. Other open field tests used the 10-min procedure.

Rotarod

On the first two days, mice were placed on a rotarod apparatus that accelerates 5-20 revolution per minute (r.p.m) for 5 min, and trained to maintain its balancing walking. On the third day, rod accelerated 5-40 r.p.m. and mice were tested twice with a maximum time of 300 s. The latencies of animals to fall off were recorded.

Balance beam

To assess sensorimotor control, we used the balance beam test as described previously (*36*). Two types of 1-meter long beams were used: 6 mm, 12 mm in width. This test contained 3 consecutive days: 2 days for training and 1 day for testing. On the first 2 days, each mouse was encouraged to cross the 12-mm beam for 3 times, and 6-mm beam for 3 times with minimal 10-min intervals. On the test day, two successful trials for each beam (without stop) were analyzed and videotaped (for further off-line analysis). The duration to cross the center 80 cm was measured.

Tail suspension test

A mouse was suspended by the tail from a lever, and the movement of the animal was videotaped for 6 min. The duration of immobility during the last 3 min was analyzed by an observer blinded to the treatment.

Forced swimming test

The forced swimming test was performed as described previously (*37*). Animals were placed in a polystyrene cylinder (20-cm high and 15 cm in diameter) containing water (15 cm in depth, 24-25 ℃). The animals were videotaped for 6 min. Immobility is defined as lack of swimming and minimal movement of one leg. Duration of immobility within the last 4 min of the test was scored manually in a double blind manner.

Pharmacogentic maniplations

For *in vivo* pharmacogenetic inactivation, mice that received AAV-hSyn-HA-hM4D-IRES-mCitrine or AAV-hSyn-EGFP in the PBN were injected with Clozapine N-oxide (CNO, 1 mg/kg, i.p.), and their behaviors were tested 30-45 min after the CNO injection.

Analysis of the scratching behavior

To measure the scratching behavior, we recorded the movement signals of the hindpaw with the magnetic induction method. A large amplitude fluctuation was observed when the mouse moves its right hindpaw implanted with a small magnet. The fluctuation signals come from both scratching and other hindpaw movements (e.g. walking, jumping). Scratching behavior induced a burst of current fluctuation exhibiting periodic characteristics, with each cycle corresponding to one hindpaw movement, referred hereafter as the scratching event. Several continuous scratching events correspond to a behavioral scratching bout. To detect scratching behavior, we analyzed the motion signal with customized program. The fluctuations larger than 3 times of the standard deviation of the whole motion signal were taken as motion

events and the time points of the peaks of motion events were taken as motion event time. We performed Fourier transform to the motion signal during scratching. The motion events caused by scratching have different temporal structure from the motion events caused by other movements. To pick up scratching events, we first took all motion events as potential scratching events. After we picked up the time point of each potential scratching event, the distribution of inter-scratching-event-interval (ISEI) was calculated. We found the distribution of ISEI had bimodal distribution in log scale. In the bimodal ISEI distribution, two peaks were located at 65 ms and 723 ms, which represented the average interval between scratching events in one scratching bout and the average interval between scratching bouts respectively. The lowest value between two peaks located at 216 ms and most of ISEI (96%) was smaller than 2 seconds. Based on the above analysis and a previous report (*31*), we applied the following criteria to extract scratching behavior from mice's motion signal: 1) The interval between two contiguous scratching events should be 0.02-0.2 s (5-50 Hz). 2) A scratching bout should contain at least 3 scratching events. The motion events caused by other hindpaw movements (e.g. walking, jumping) were mostly excluded by applying these criteria. A cluster of scratching bouts with interval less than 2 seconds was defined as a scratching train. Manual adjustment was performed by customized graphical user interface program to pick up missed scratching events and delete false scratching events. The number of scratching bouts was then calculated automatically.

Immunofluorescence staining

Mice were anesthetized with overdose of pentobarbital sodium, and perfused transcardially with saline followed by PBS buffer containing 4% paraformaldehyde (PFA). Brains or spinal cord were dissected, and post-fixed overnight at 4 ℃ in 4% PFA, followed by cryoprotection in 30% sucrose in PBS at 4 ℃. Free-floating sections (30 μm) prepared with a cryostat were used for immunohistochemical staining. Tissue sections were blocked for 30 min at room temperature in PBST (0.3% Triton X-100) with 5% normal donkey serum, followed by incubation with primary antibodies at 4 ℃ overnight and secondary antibodies at room temperature for 2 hr. Primary antibodies used in immunohistochemistry (IHC) experiments were rabbit anti-c-Fos (1:2000, Santa Cruz, sc-52), rabbit anti-c-Fos (1:20000, Synaptic System, 226003), rabbit anti-DsRed (1:500, Abmart, 632496), guinea pig anti-NeuN (1:1000, Millipore, ABN90), rabbit anti-GFP (1:500, Life Technology, A11122), mouse anti-GFP (1:500, Life Technology, A11120), Alexa 405 conjugated streptavidin protein (1:500, Invitrogen, S32351). Secondary antibodies were donkey anti-rabbit IgG-Alexa 488 (1:250, Jackson ImmunoResearch Laboratories, 711-545-152), donkey anti-mouse IgG-Alexa 488 (1:250, Jackson ImmunoResearch Laboratories, 715-545-150), donkey anti-rabbit IgG-Cy3 (1:250, Jackson ImmunoResearch Laboratories, 711-165-152), donkey anti-mouse lgG-Cy3 (1:250, Jackson ImmunoResearch Laboratories, 715-165-150), donkey anti-guinea pig IgG-Cy3 (1:250, Jackson ImmunoResearch Laboratories, 706-165-148).

Images were taken using a fluorescence microscope, Neurolucida microscope, confocal microscope or Nikon NiE-A1 plus confocal microscope. Cell counting was carried out manually using Fiji (NIH). For examining the c-Fos expression in spinal cord or PBN, the pruritic compounds were injected 2-2.5 hr prior to the perfusion.

Immunohistochemical staining

Floating sections were washed in PBS, quenched in 0.3% H_2O_2/PBS for 30 min, and blocked for 2 hr at room temperature in PBST with 1% goat serum. Then the sections were incubated with rabbit anti-c-Fos (1:2000, Santa Cruz, sc-52) at 4 ℃ overnight. After washing in PBS, the sections were incubated with biotinylated goat anti-rabbit IgG antibody (1:1000, Jackson ImmunoResearch Laboratories, 111-065-003) for 1.5 hr. The sections was then washed and incubated with avidin-biotin-peroxidase complex (Vector Laboratories, 1:500 for Reagent A and B each in PBS) for 30 min at room temperature. To reveal the horseradish peroxidase , the sections were exposed to the 3,3'-diaminobenzidine (DAB)-ammonium nickel sulfate reaction buffer for 1-3 min. The sections were then dehydrated in a series of ethanol solutions of incremental concentrations (50%, 75%, 100%) and cleared in dimethylbenzene (5 min), coverslipped with quick-hardening mounting medium.

Images were taken with Neurolucida microscope. Images at three coronal sections (bregma -5.02, bregma -5.20, bregma -5.34 mm) were processed under the same adjustment. Cell counting was carried out manually using Fiji (NIH). c-Fos^{+} neurons are marked in both contralateral and ipsilateral PBN, including lateral PBN (LPBN), medial PBN (MPBN) and the Kolliker-Fuse nucleus (KF).

In situ **hybridization**

In situ hybridization was performed as previously described (*38*). *Gad1*, *Vglut1*, *Vglut2*, *Vglut3*, *GRP* and *SST* probes were used. Briefly, all probes were made using digoxigenin (DIG)-labeled nucleotides. The slides were heated at 60 ℃ for 1 hr, fixed in 4% Diethyl Pyrocarbonate (DEPC)-PFA for 20 min, and washed in DEPC-PBS 2 x 5 min. The tissue was treated with proteinase K (10 μg/ml) for 12 min, and washed in DEPC-PBS for 5 min, then fixed with 4% DEPC-PFA for 20 min. The tissue was rinsed once in DEPC-H_2O, followed by acetylation in triethanolamine-HCl with 0.25% acetic anhydride for 8 min, and the tissue was then washed in DEPC-PBS for 5 min. The tissue was prehybridized for 3-5 hr at 65 ℃ in hybridization buffer. After prehybridization, the tissue was hybridized in hybridization buffer containing a probe with a final concentration of 1 μg/ml for 12-16 hr. Series of washes were performed sequentially at 65 ℃ in pre-warmed buffers: 1 x10 min in 1X SSC, 1 x10 min in 1.5 X SSC, then the tissue was washed at 37 ℃: 2 x 20 min in 2 X SSC buffer, followed by treatment with RNase A (3 μg/ml) in 2 X SSC for 30 min, and washed 1 x 10 min in 2 X SSC at room temperature. Next, the tissue was washed at 65 ℃ in pre-warmed buffers: 2 x 30 min in 0.2 X SSC buffer, and the tissue was further washed at room temperature with 0.2 X SSC buffer and PBST each for 15 min. The tissue was then incubated in blocking buffer (20% heat-inactivated sheep serum in PBST) for another 1-3 hr, followed by incubation with sheep anti-DIG-AP (1:2000 in PBST with 1%

heat-inactivated sheep serum) overnight at 4 ℃. The next day, after washing 3 x 10 min in PBST and 2 x 10 min in AP buffer (100 mM Tris-Cl, 100 mM NaCl, 0.1% TWEEN 20, 50 mM $MgCl_2$), sections were visualized in AP buffer containing NBT and BCIP. AP buffer that containing (for every ml): 1 μl of NBT (75 mg/ml) and 3.5 μl of BCIP (50 mg/ml) were used for developing. The tissue was let to develop in the dark for 2-20 hr.

Fluorescence *in situ* hybridization and immunofluorescence double staining

To determine the colocalization of c-Fos with *Vglut2* and *Gad1*, fluorescence *in situ* hybridization and immunofluorescence double staining was performed. Mouse was first perfused with saline followed by 4% PFA in PBS, and post-fixed in 4% PFA overnight. The next day, the brain tissue was washed in 0.01 M PBS for 3 times, and then embedded in 3% BactoAgar/PBS. The brain was sectioned at 40 μm with a vibratome, and the sections were collected into cold DEPC-PBS. Floating sections were washed once in DEPC-PBS and twice in DEPC-PTW (PBS-Tween, PBS with 0.1% Tween-20) each for 5 min. Then, the brain sections were washed in 2 X SSC containing 0.5% Triton X-100 for 30 min, followed by another round of DEPC-PTW washing. After acetylation for 10 min in 0.1 M triethanolamine (pH 8.0) with 0.25% acetic anhydride (vol/vol), the sections were pre-hybridized with hybridization buffer for 3 hr at 65 ℃. The sections were then hybridized with hybridization buffer with *Vglut2* and *Gad1* probe at a final concentration of 0.5 μg/ml for 16-18 hr at 65 ℃. After hybridization, sections were rinsed in pre-hybridization solution and pre-hybridization solution/TBST (TBS-Tween TBS with 0.1% tween-20) mixture (vol/vol, 1:1), 30 min for each. Next, the sections were washed with TBST for twice and Tris-acetate-EDTA buffer (TAE) for three times, each for 5 min. The sections were transferred wells in 2% agarose/TAE gel, and run gel at 60 V for 2 hr. The sections were then washed twice in TBST, and subsequently incubated with sheep anti-DIG-AP (1:1000) and rabbit anti-c-Fos antibody (1:5000, Merck/Calbiochem) in 0.5% blocking reagent (Roche, 11096176001) at 4 ℃ overnight. On the second day, the sections were washed three times in AGT buffer (0.5% FBS, 0.1% Triton X-100, 2 mM $MgCl_2$ in 0.01 M PBS) for 30 min and incubated with donkey anti-rabbit IgG-Alexa 488 (1:250, Jackson ImmunoResearch Laboratories) in PBS for 2 hr at room temperature. The sections were washed three times in Tris-HCl (100 mM, pH8.0) for 5 min and visualized with fast red solution [dissolve 1 fast red tablet in 2 ml of Tris-HCl (100 mM, pH8.0)] for 3 hr.

Brain slice electrophysiology

Slice electrophysiology were performed as described previously (*39*). Mice were anesthetized with isoflurane and perfused transcardially with an ice-cold cutting solution containing (in mM) sucrose 213, KCl 2.5, NaH_2PO_4 1.25, $MgSO_4$ 10, $CaCl_2$ 0.5, $NaHCO_3$ 26, and glucose 11 (300-305 mOsm). The brain was rapidly dissected, and coronal slices (250 μm) were sectioned in the ice-cold cutting solution, using a vibratome at slicing speeds of 0.14 mm/s and a blade vibration amplitude of 1 mm. Slices were transferred to the holding chamber and incubated in 34 ℃ artificial

cerebral spinal fluid containing (ACSF, in mM) NaCl 126, KCl 2.5, NaH_2PO_4 1.25, $MgCl_2$ 2, $CaCl_2$ 2, $NaHCO_3$ 26, and glucose 10 (300-305 mOsm) to recover for 40 min. The slices were then kept at room temperature prior to recordings. Both cutting solution and ACSF were continuously bubbled with 95% O_2/5% CO_2.

Slices were placed on glass coverslips coated with poly-L-lysine, and submerged in a recording chamber. All experiments were performed at near-physiological temperatures (32-34 °C) using an in-line heater while perfusing the recording chamber with ACSF at 3-4 ml/min using a pump. Whole-cell patch-clamp recordings were made from the target neurons under IR-DIC visualization and a CCD camera using an Olympus BX51WI microscope. The cesium-based internal solution contained (in mM) $CsMeSO_3$ 130, $MgCl_2$ 1, $CaCl_2$ 1, HEPES 10, QX-314 2, EGTA 11, Mg-ATP 2, Na-GTP 0.3 (pH 7.3, 295 mOsm). The potassium-based internal solution contained (in mM) K-gluconate 130, $MgCl_2$ 1, $CaCl_2$ 1, KCl 1, HEPES 10, EGTA 11, Mg-ATP 2, Na-GTP 0.3 (pH 7.3, 290 mOsm). Blue LED or laser was used to activate ChR2. Bath application of NBQX (10 μM) was used to examine the synaptic property (*40*).

In DREADDs experiments, neurons in the PBN were recorded in cell-attached configuration, and CNO (5 μM) was bath applied for ~ 2 min. Cell-attached recordings were obtained with pipettes (2-3 MΩ) filled with ACSF. The seal resistance was 20-100 MΩ. Recording was performed in voltage-clamp mode, and holding potential was continually monitored and adjusted to keep the holding current near 0 pA, in order to minimize any influence on the membrane potential of the recorded cell.

Spinal cord slice electrophysiology

Spinal cord slice recording was performed as described previously (*41*). Young (24-30 day-old) mice were deeply anesthetized with a mixture of 0.2 g/kg ketamine and 0.01g/kg xylazine. Cervical segments of the spinal cord were excised and transverse spinal cord slices (300 μm) were sectioned at slicing speeds of 0.06 mm/s in the ice-cold cutting solution containing (in mM) sucrose 50, KCl 1.8, NaCl 95, KH_2PO_4 1.2, $MgSO_4$ 7, $CaCl_2$ 0.5, $NaHCO_3$ 26, and glucose 15 (310-320 mOsm). Slices were transferred to the holding chamber and incubated in 34 °C ACSF containing (in mM): NaCl 127, KCl 1.8, KH_2PO_4 1.2, $CaCl_2$ 2.4, $MgSO_4$ 1.3, $NaHCO_3$ 26, glucose 15, and was oxygenated with 95% O_2/ 5% CO_2 (310-320 mM). Thirty min after recovery, the slice was then transferred into a recording chamber and perfused with oxygenated ACSF at 3 ml/min at near-physiological temperatures (32-34 °C). Patch-clamp recordings were made from lamina I EYFP[+] or beads^{+} neurons of mice under a fluorescent microscope. Whole-cell patch-clamp recordings were performed using glass pipettes with a resistance of 2-6 MΩ. The 593 nm laser-induced inhibition of beads^{+} neurons expressing eNpHR3.0 were investigated in current-clamp mode using potassium-based (K^{+}-based) internal solution. The electrophysiological properties of the GRPR^{+} neurons and the light-evoked post synaptic responses in beads^{+} neurons were investigated in voltage- and current-clamp modes using K^{+}-based and cesium-based (Cs^{+}-based) internal solution respectively. The K^{+}-based internal solution contained (in mM): K-gluconate 130, $MgCl_2$ 1, $CaCl_2$

1, KCl 1, HEPES 10, EGTA 11, Mg-ATP 2, Na-GTP 0.3 (pH 7.3, ~295 mOsm). The Cs^+-based internal solution contained (in mM): $CsMeSO_3$ 130, $MgCl_2$ 1, $CaCl_2$ 1, HEPES 10, QX-314 2, EGTA 11, Mg-ATP 2, Na-GTP 0.3 (pH 7.3, ~295 mOsm). In most experiments, 0.2% biocytin was included in the internal solution.

Extracellular recording

To record the *in vivo* activity of PBN neurons during scratching behavior, self-made multi-channel electrodes were implanted into the PBN. Mice (8-10 weeks old) were anesthetized with pentobarbital sodium (0.1 g/kg) and mounted in a stereotaxic apparatus. Lidocaine was applied before incision. Craniotomy was performed to implant multi-channel electrodes. Right PBN was targeted at location 0.5-1.5 mm posterior to Lamda point, 1.0-1.5 mm lateral from midline. The electrode was tilted 10 degree anteriorly to avoid a blood vessel, and inserted 2.9-3.1 mm ventrally from the brain surface. Five skull screws were implanted around the site of craniotomy. Reference and ground wires were connected to the screws. After insertion, the lower part of electrode was fixed by dental cement, and the upper part of electrode wires was bended after lower part dental cement was completely solid. This helps alleviating the vibration caused by plugging or unplugging the connector. Then dental cement was used to fix the whole electrode to the skull. Lidocaine was applied to mice's left hindpaw, and a magnet (1 mm in diameter, 3 mm in length) was implanted for monitoring the scratching behavior. After injection of antibiotics (Ceftriaxone sodium, 0.1 g/kg), mice were allowed for one week to recover from surgery before recording.

During recording, the multi-channel electrode was connected with a 64-channel system through the head-stage, and the mouse was put in a chamber, which was surrounded by a coil, for 1-3 hours before recording. Then the mouse was injected with pruritogens intradermally to the left side of nape, and placed back in the chamber for recording. The signal for behavior was amplified with an amplifier, and fed into the data collection unit, which was used to collect neural data and behavior data simultaneously. The neural signal was amplified and highpass filtered at 250 Hz and sampled at 30 kHz to record the action potential signal. The movement signal was lowpass filtered at 250 Hz and digitized at 2 kHz. This protocol was performed for every mouse with different pruritogens. For each mouse, the time interval between two experiments with different pruritogens was at least 24 hr. The sequences of pruritic drugs were randomized for each mouse. In total, 28 mice were implanted with electrodes and used for data collection.

To visualize the location of the electrode, the mice were deeply anesthetized and direct current (25 μA, 15-20 s) was applied to each channel of the electrode to mark the electrode location. Then animals were perfused with saline followed by chilled 4% PFA solution and dehydrated with 30% sucrose solution. After fixation, the brain was sectioned into 50-μm sections to check the location of electrode tips. Only data from mice with all electrodes within the PBN were included for analysis. We obtained 13 mice with all electrodes located in the PBN.

Extracellular recording data analysis

Spikes recorded were sorted with Offline Sorter using cluster analysis of principal components and waveform amplitudes. Then analysis was performed using MATLAB. Neural activity referenced to scratching behavior (the start of scratching bout, the end of scratching bout) was averaged in 70-ms bins, shifted by 10 ms and averaged across trials to construct peri-stimulus time histogram (PSTH). Experiments, with the number of scratching bouts larger than 10, were included in the analysis. Cells with firing rate larger than 1 Hz were included in the analysis.

If a given cell has significant responses to itch related behavior, it would display more reliable response across different trials. So for the evaluation of significant responses, between-trial and within-trial correlation coefficients were calculated. The responses were separated along time into two sections. Between-trial correlations were calculated as the correlation of responses to different sections. Within-trial correlations were calculated as the correlation between all trials in the same section, which quantify the response reliability. We compared the average between-trial and within-trial correlation coefficient. Only cells that have significantly higher within-trial correlation coefficient ($P < 0.01$, Wilcoxon signed rank test) than between-trial correlation coefficient were considered responsive (*42*).

For the arrangement of cells according to their maximum firing rate, PSTH of each cell was normalized by Z-Score, and then the time of the maximum firing rate was determined. Cells were sorted according to the time of the maximum firing rate from earliest to latest.

Fiber photometry

The optical fibers were implanted in the PBN one week after the viral injection, and the animals were allowed to recover for a week before recording. The mice were handled for 3 days prior to fiber photometry recording. The scratching behavior and Ca^{2+} transient (or EGFP) signal were recorded simultaneously with F-scope-G-2 after intradermal injection of histamine or chloroquine into right side of the nape.

In order to monitor the neuronal activity of PBN neurons in response to optogenetic activation of spinal GRPR$^+$ neurons, GRPR-iCreERT2 mice were injected with AAV-EF1α-DIO-ChR2(H134R)-EYFP into right dorsal horn of spinal cord. After recovery for one week, mice were injected with tamoxifen daily for three successive days. One week later, mice were injected with AAV-hSyn-GCaMP6s in the left PBN. Mice were allowed to recover for one week before implantation of optical fibers into left PBN and attaching LED (470 nm) to cervical spinal cord. For implantation of LED, cervical vertebrae were exposed, and wireless LED covering the dorsal spinal cord injected with AAV-EF1α-DIO-ChR2(H134R)-EYFP was attached to the cervical vertebrae with dental cement. The magnet was implanted into the right hindpaw.

Fiber photometry and scratching behavior data were analyzed using MATLAB. After subtracting noise signal of fiber photometry recording system, we smoothed the data with a moving average filter (20-ms span). The values of Ca^{2+} transients change

($\Delta F/F$) from 3.5 s preceding scratching train onset to 5 s after scratching train onset were derived by calculating $(F\text{-}F_0)/F_0$ for each scratching train, where F_0 is the median Ca^{2+} transients from 3.5 s preceding scratching train to scratching train onset. $\Delta F/F$ values of all scratching trains were then averaged and plotted with a shaded area indicating SEM.

Statistical analysis

Statistical analysis was performed using Igor Pro, Prism 6 and MATLAB 2013b. The data were analyzed using unpaired t-test, paired t-test, one-way ANOVA with Bonferroni's correction for multiple comparisons, two-way ANOVA, Wilcoxon signed rank test and Kolmogorov-Smirnov test. The cutoff for significance was held at $P = 0.05$.
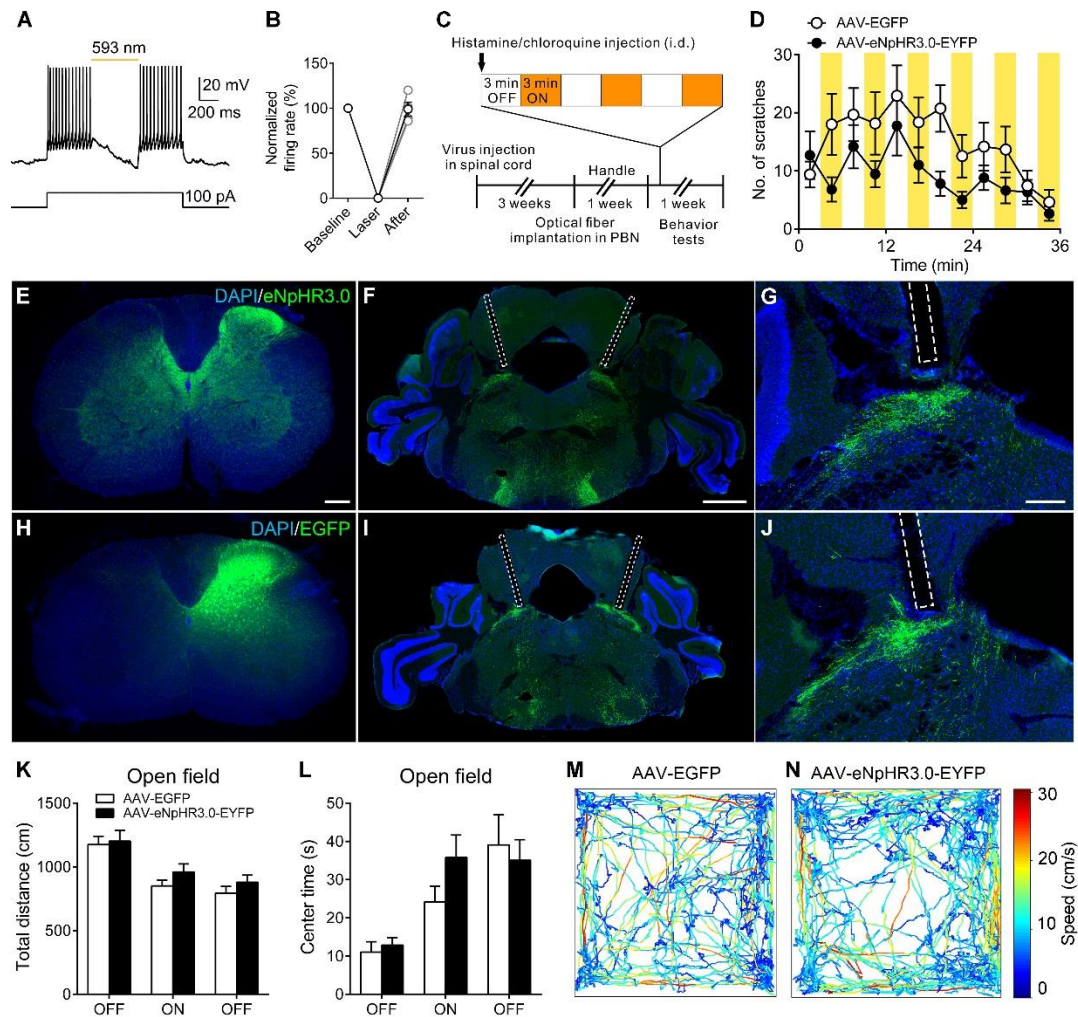
Fig. S1. Effect of photoinhibition of the spinoparabrachial pathway on mouse behavior.

(**A**) Illumination with 593 nm laser potently inhibited firing of retrogradely labeled spinoparabrachial neurons that express eNpHR3.0$^+$. Neurons were injected with 100-pA current step for 1500 ms to evoke robust spike firing. Yellow bar indicates the delivery of 593 nm laser. (**B**) Normalized firing rate of beads$^+$/eNpHR3.0$^+$ neurons were analyzed for 500 ms before, during and after laser periods (n = 4 neurons). (**C**) Timeline of the behavioral experiments and paradigm of optogenetic manipulation of the spinoparabrachial pathway. (**D**) Effect of optogenetic inhibition of spinoparabrachial pathway on scratching behavior of mice that received intra-spinal injection of AAV-EGFP or AAV-eNpHR3.0-EYFP in response to chloroquine (n = 16-17, yellow shade indicates constant 593 nm laser stimulation). (**E**, **H**) Example graphs showing expression of the AAV-eNpHR3.0-EYFP (**E**) and AAV-EGFP virus (**H**) in the spinal cord. Scale bar, 200 μm. (**F**, **I**) Example graphs showing the distribution pattern of EYFP$^+$ (**F**) and EGFP$^+$ fibers (**I**) in the PBN. The dashed lines outlined the position of optical fibers. Scale bar, 1 mm. (**G**, **J**) Enlarged images showing the distribution of the EYFP$^+$ (**G**) and EGFP$^+$ fibers (**J**) in PBN. The dashed lines outlined the position of optical fibers. Scale bar, 200 μm. (**K**, **L**) Effect of

14

optogenetic inhibition of spinoparabrachial pathway on locomotor activity tested by open field test (n = 16-17). (**M, N**) Example traces of open field test for AAV-EGFP (**M**) and AAV-eNpHR3.0-EYFP group (**N**). Error bars represent SEM.
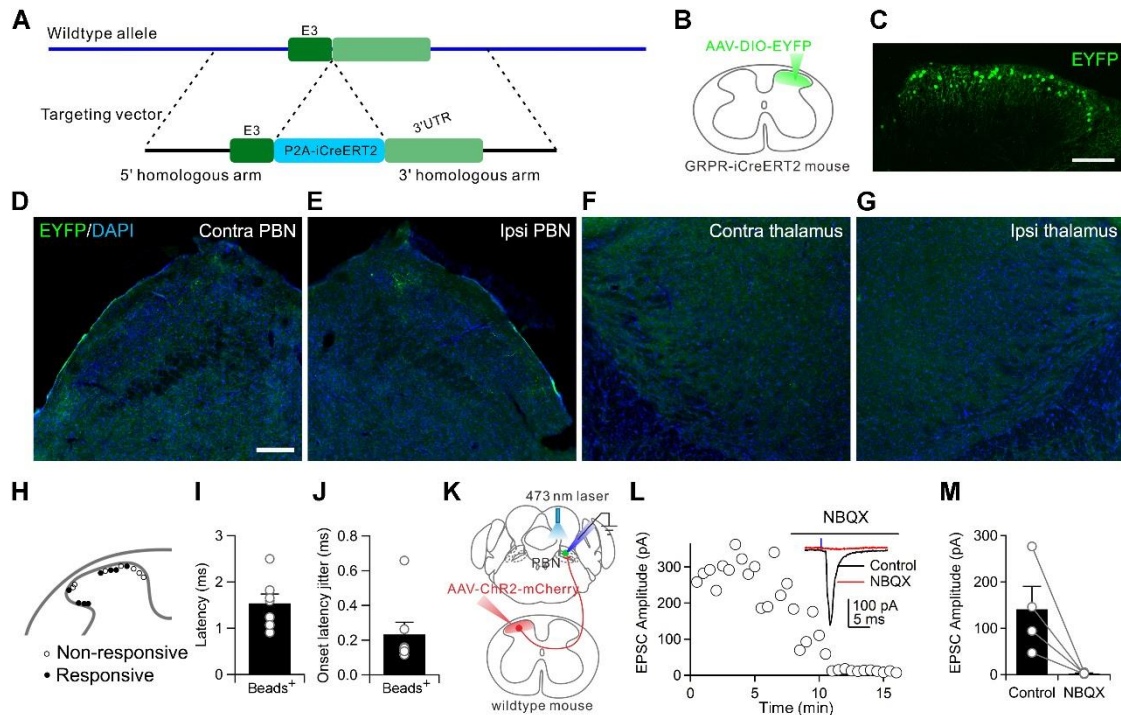
Fig. S2. Connection between spinal neurons and the PBN.

(**A**) Targeting strategy for generating the GRPR-iCreERT2 mouse line. (**B**) Schematic diagram showing the injection of AAV-DIO-EYFP virus into the dorsal spinal cord of GRPR-iCreERT2 mice. (**C**) Distribution of EYFP$^+$ neurons in the superficial spinal cord of GRPR-iCreERT2 mice injected with AAV-DIO-EYFP in the spinal cord. Scale bar, 100 μm. (**D**, **E**) Distribution of EYFP$^+$ fibers in the contralateral and ipsilateral of PBN of GRPR-iCreERT2 mice injected with AAV-DIO-EYFP in the spinal cord. Scale bar, 200 μm. Contra, contralateral; Ipsi, ipsilateral. (**F**, **G**) Distribution of EYFP$^+$ fibers in the contralateral and ipsilateral of ventral posterior thalamus of GRPR-iCreERT2 mice injected with AAV-DIO-EYFP in the spinal cord. (**H**) Plot of the locations of the recorded neurons in the dorsal spinal cord (open circle, non-responsive; solid circles, responsive with EPSC). (**I**) Summary plot showing latency of light-evoked EPSCs in response to activation of GRPR$^+$ neurons and their axons ($n = 7$). (**J**) Summary plot showing EPSC latency jitter ($n = 7$). (**K**) Schematic diagram of the slice recording in the PBN one month after the AAV-ChR2-mCherry virus was injected into the dorsal spinal cord of wild-type mice. (**L**) An example graph showing amplitude of EPSC recorded in the PBN evoked by photostimulation of spinal projection axons (473 nm, 1 ms) before and during bath application of NBQX (an AMPA receptor antagonist, 10 μM). Inset: the light-evoked EPSC before (black) and after bath application of NBQX (red). (**M**) Summary graph showing the amplitude of light-evoked EPSCs in the PBN before and after application of NBQX ($n = 4$ cells), $P = 0.066$, paired t-test. Error bars represent SEM.

16
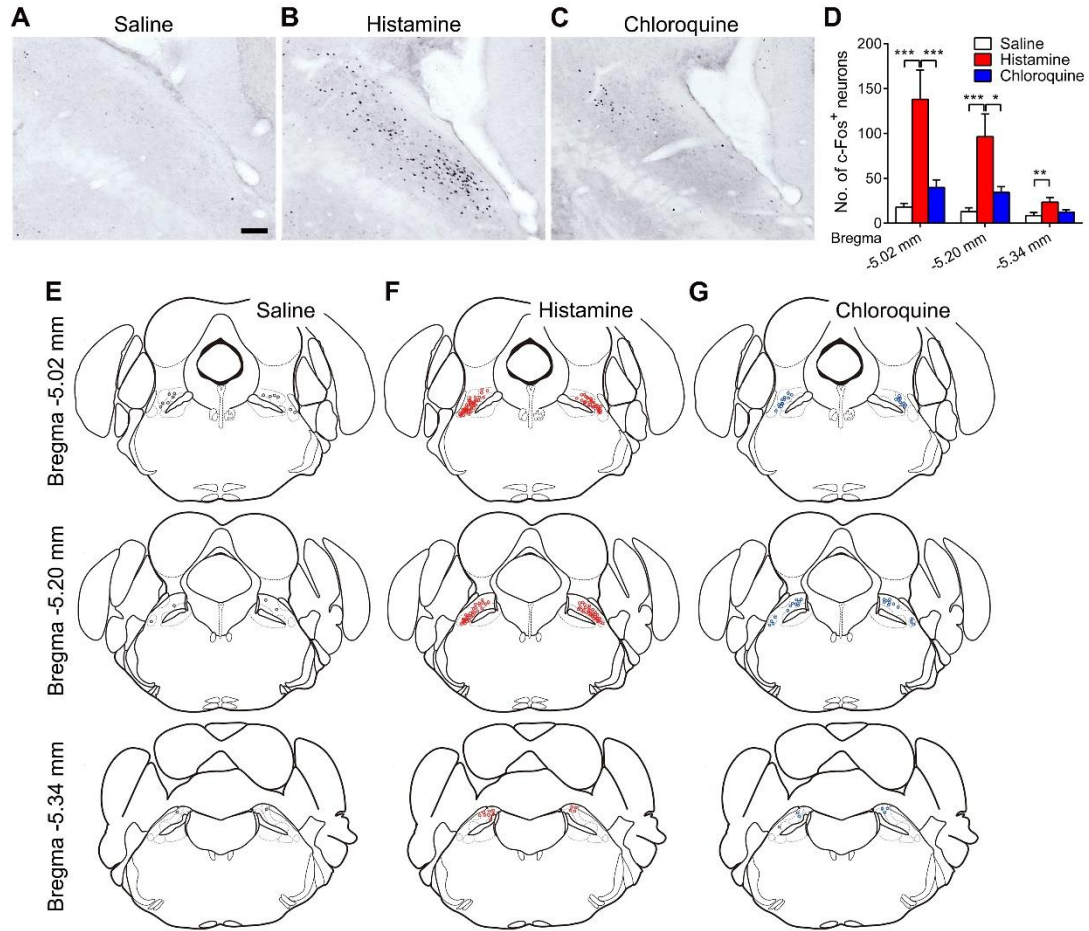
Fig. S3. c-Fos expression in the PBN after intradermal injection of pruritogens.
(**A**-**C**) Bright field micrographs showing c-Fos$^+$ neurons in the PBN 2.5 hours after intradermal injection of saline (**A**), histamine (500 μg/50 μl, **B**), or chloroquine (200 μg/50 μl, **C**). Scale bar, 100 μm. (**D**) Graph showing the number of c-Fos$^+$ neurons in the PBN induced by intradermal injection of saline, histamine and chloroquine (n = 3-5 mice for each group). (**E**-**G**) Schematic plot of c-Fos$^+$ neurons on coronal sections of PBN. Each open circle represented 3 c-Fos$^+$ neurons. c-Fos$^+$ neurons outside of PBN were not analyzed or plotted. Error bars represent SEM. *P < 0.05, **P < 0.01, ***P < 0.001, one-way ANOVA with Bonferroni's correction for multiple comparisons test for **D**.
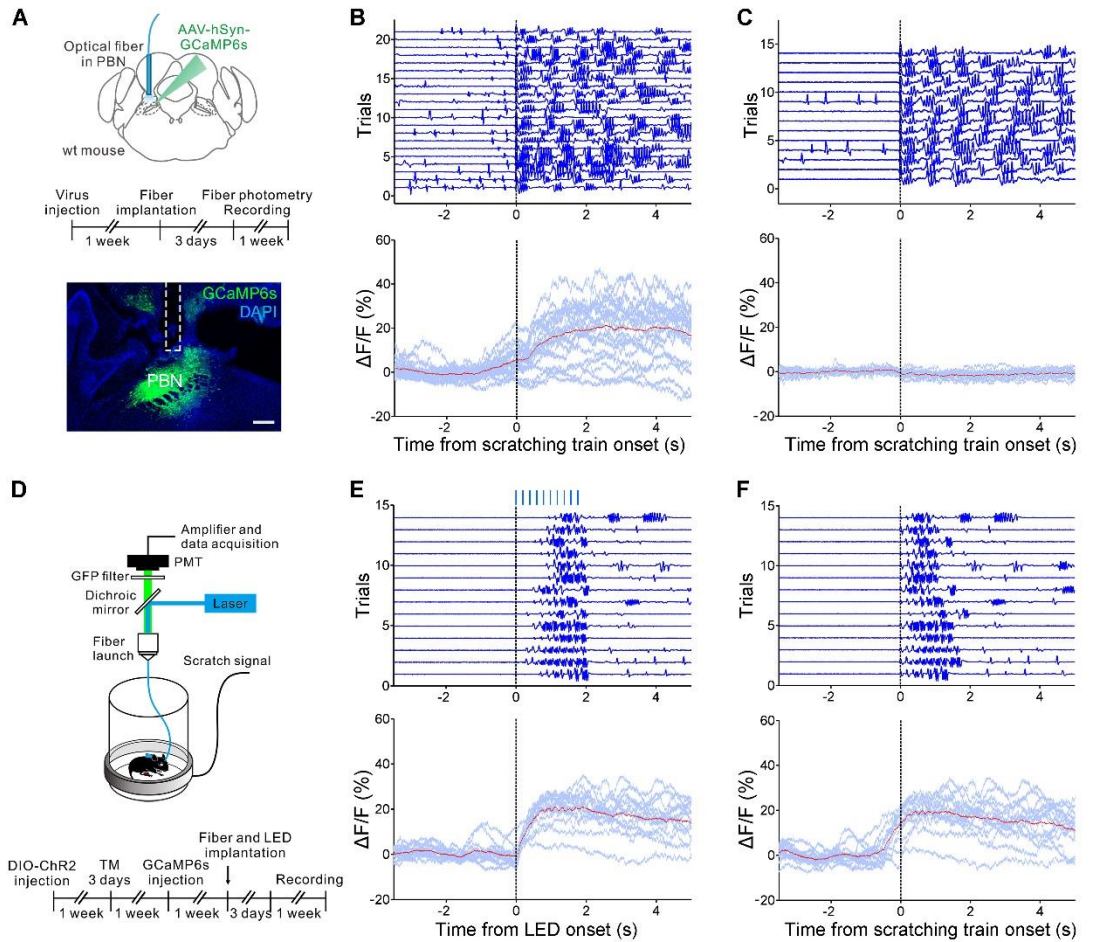
Fig. S4. Determine the activity of PBN neurons during itch processing with fiber photometry.

(**A**) Top: schematic showing the viral injection and fiber implantation. Middle: experimental timeline. Bottom: a representative image showing the expression of GCaMP6s for a mouse injected with AAV-hSyn-GCaMP6s and implanted with optical fiber (outlined by dashed lines) in the PBN. Scale bar, 200 μm. (**B**) A representative experiment showing the Ca^{2+} transients associated with scratching behavior induced by intradermal injection of chloroquine in a mouse injected with AAV-hSyn-GCaMP6s in the PBN. Top, the scratching behavior aligned to the beginning of each scratching train. Each row represents a scratching train. Bottom, the Ca^{2+} transients associated with individual scratching train aligned according to the beginning of scratching behavior (blue). The red trace represents the average of all traces for Ca^{2+} transients. (**C**) A representative experiment showing fluorescent signal for EGFP in the PBN during scratching behavior induced by intradermal injection of chloroquine. Top, the scratching behavior aligned to the beginning of scratching trains. Each row represents a scratching train. Bottom, the fluorescent signal for EGFP associated with individual scratching train aligned according to the beginning of scratching behavior (blue). The red trace represents the average of all traces for EGFP signal. (**D**) Top: schematic depicting the recording system for obtaining the Ca^{2+}

18

signal and scratching behavior induced by optogenetic activation of spinal GRPR$^+$ neurons with wireless LED. Bottom: experimental timeline for examining the PBN neuronal activity using GRPR-iCreERT2 mice injected with AAV-DIO-ChR2-EYFP in the right dorsal spinal cord and AAV-hSyn-GCaMP6s in the left PBN. TM: tamoxifen. (**E**, **F**) A representative experiment showing the Ca^{2+} transients in the PBN induced by optogenetic activation of GRPR$^+$ neurons in a GRPR-iCreERT2 mouse. LED pulses (470 nm, 1 ms, blue bars) were delivered at 5 Hz for 2 seconds. (**E**) Top: the scratching behavior aligned to the onset of each train of LED pulses. Each row represents a trial. Bottom: the Ca^{2+} transients aligned according to the onset of LED pulses (blue). The red trace represents the averaged Ca^{2+} signal. (**F**) Top: the scratching behavior aligned to the onset of each scratching train. Bottom: the Ca^{2+} transients aligned according to the onset of scratching train (blue). The red trace represents the average of all Ca^{2+} traces. Similar results were obtained from another two mice.
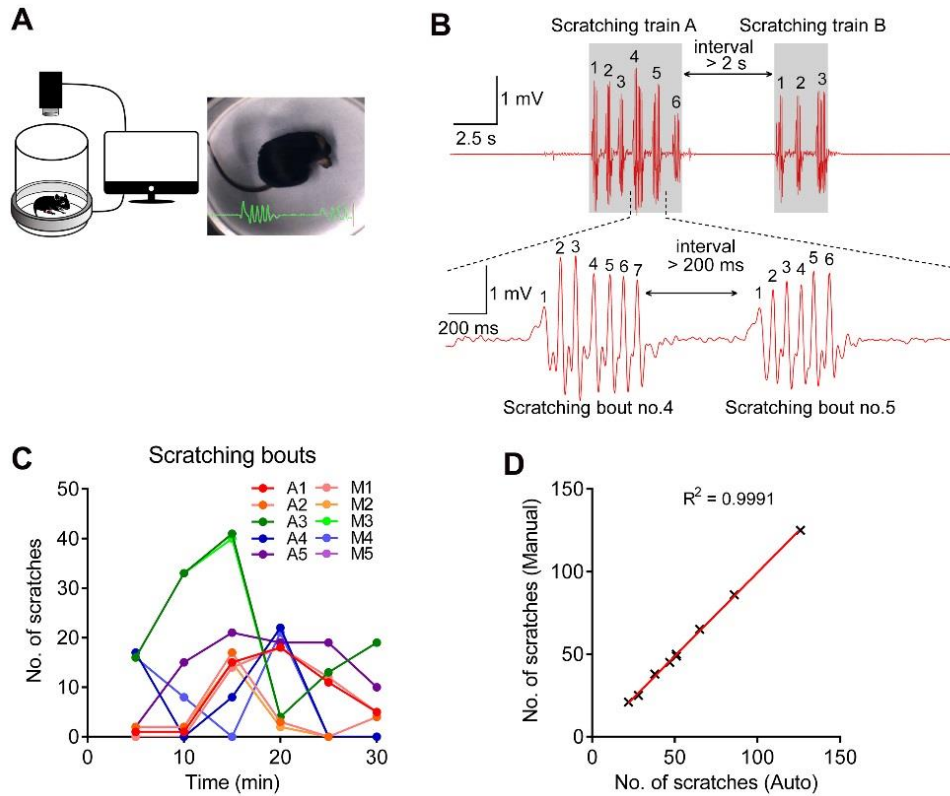
Fig. S5. Recording of the mouse scratching behavior with a magnetic induction method.

(**A**) Schematic showing the recording of scratching behavior with a high-speed camera and a magnetic induction method simultaneously. (**B**) A representative trace of mouse's scratching behavior recorded with the magnetic induction method, with scratching train A consisting of 6 scratching bouts and scratching train B consisting of 3 scratching bouts. There were 7 scratching events in the fourth scratching bout and 6 scratching events in the fifth scratching bout. (**C**) Comparison of automatic counting of scratching bouts of 5 mice after intradermal injection of histamine (500 μg/50 μl) with results from manual analysis of the video recording in 5-min bins. (**D**) Linear regression analysis correlating the number of scratching bouts analyzed by automatic counting and scratching bouts counted manually ($n = 9$ mice).
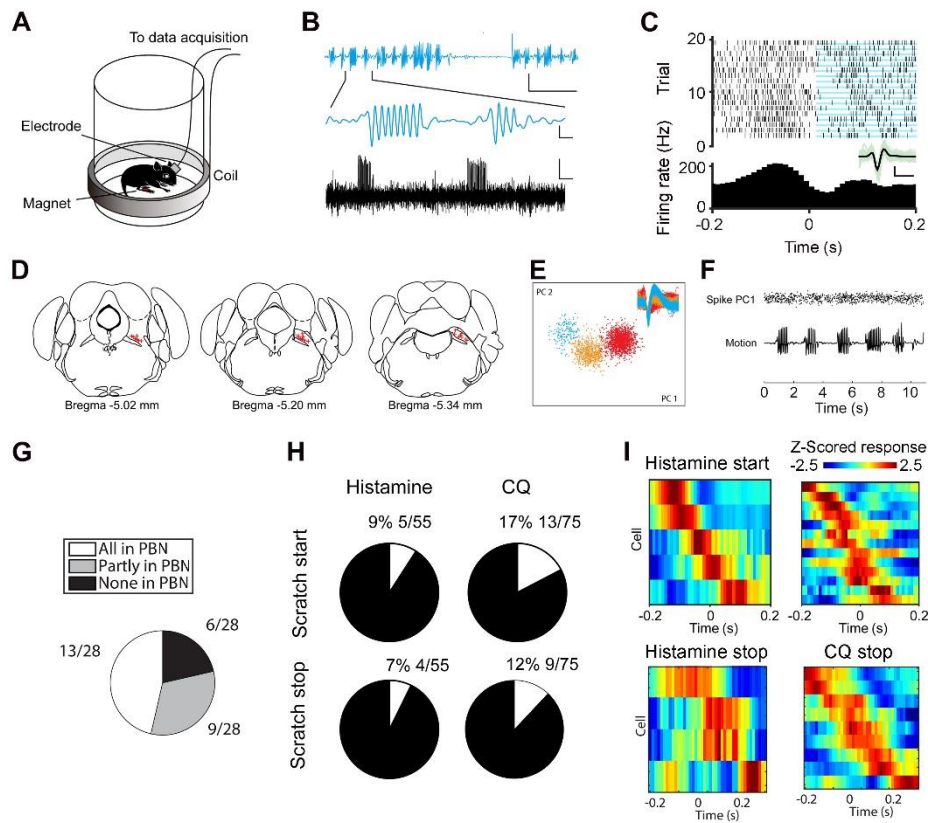
Fig. S6. *In vivo* **extracellular recording of neuronal activity of the PBN.**

(**A**) Schematic depicting the recording system for obtaining neural and motion signal simultaneously. A magnet was implanted into the hindpaw of mice, and the current induced by the movement of the magnet in the coil was recorded. Neural signal was obtained by implanting a multi-electrode in the PBN. (**B**) Example traces of hindpaw motion (blue) and neural signal (black). Scale bars: top, 1.5 mV, 5 s; middle, 500 μV, 200 ms; bottom, 100 μV, 200 ms. (**C**) Response of an example cell aligned to the beginning of the scratching bouts in response to intradermal injection of chloroquine (200 μg/50 μl, i.d.). Scratching bouts were indicated by blue shade. Black trace, averaged spike waveform. Scale bars, 50 μV, 1 ms. (**D**) The locations of electrodes implanted in animals with correct implantation sites. Each red cross indicates one penetration in one animal. (**E**) Clustering of units by principal component analysis. (**F**) Upper black dots represent the first principal component of spike waveforms. Lower trace shows the animal's movement amplitude at the same time. Spike waveforms remain stable during the movement. (**G**) Summary showing the implantation of electrode. (White: all channels were located in the PBN. Gray: some channels of the electrode were located in the PBN. Black: All channels were outside of PBN.) (**H**) Proportion of cells with significant responses during animal scratching. (White: responsive cells. Black: non-responsive cells). (**I**) The sequential firing of responsive cells at the beginning or end of the scratching bout in histamine and chloroquine (CQ) models. Cells' firing were z-scored and sorted according to the time of maximum firing rate.
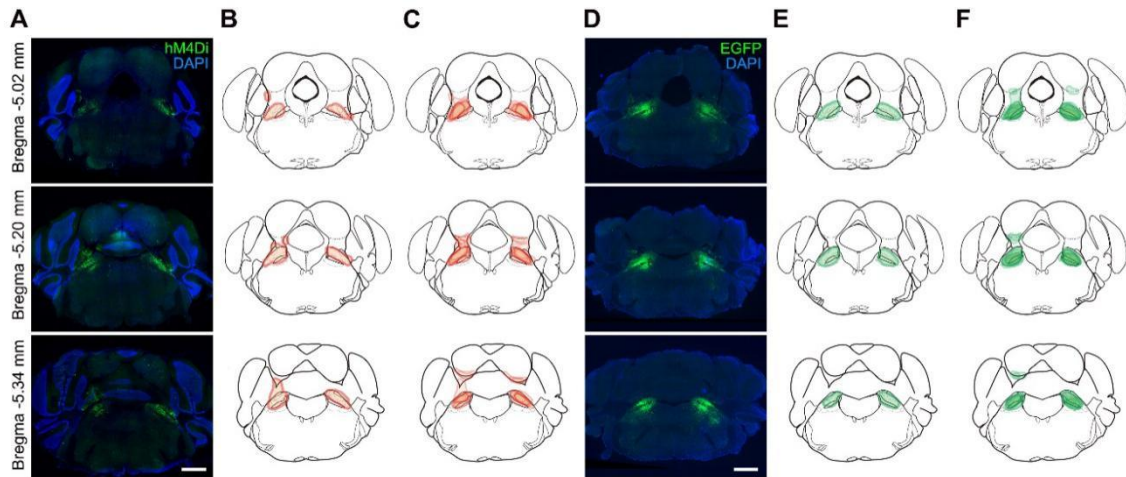
Fig. S7. Virus infection areas in the PBN of animals in AAV-hM4Di-mCitrine and AAV-EGFP group.

(**A**) Representative images from a mouse injected with AAV-hM4Di-mCitrine virus in the PBN. Scale bar, 1 mm. (**B**) Depiction of virus infection area according to the fluorescent images in **A**. (**C**) Super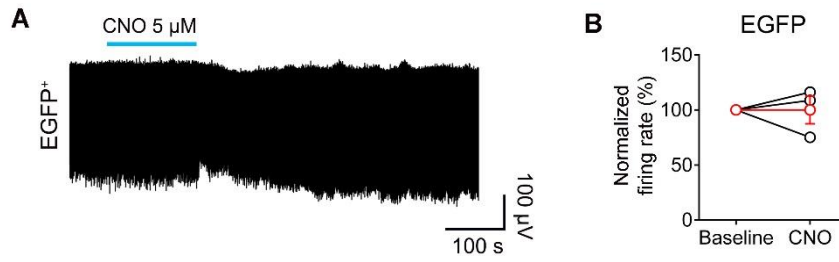imposed depiction of virus infection area for 8 mice in AAV-hM4Di-mCitrine group. (**D**) Representative images from a mouse injected with AAV-EGFP virus in the PBN. Scale bar, 1 mm. (**E**) Depiction of virus infection area according to the fluorescent images in **D**. (**F**) Superimposed depiction of virus infection area for 6 mice in AAV-EGFP group.

Fig. S8. Effect of CNO on EGFP⁺ neurons in the PBN.

(**A**) An example experiment showing that bath application of CNO (5 μM) did not change the firing rate of the EGFP⁺ neuron recorded in cell attached mode in the PBN of mice injected with AAV-EGFP in the PBN. (**B**) Summary graph showing the effect of CNO on the firing rate of the EGFP⁺ neurons in the PBN ($n = 3$ neurons).
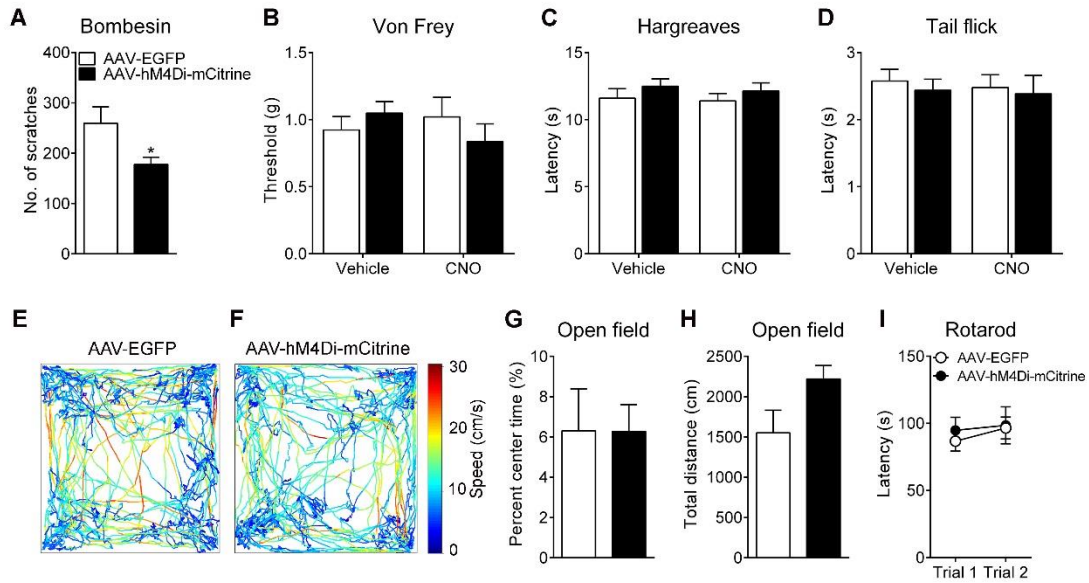
Fig. S9. Effect of pharmacogenetic suppression of the PBN on mouse behavior.
(**A**) Effect of CNO (1 mg/kg, i.p.) on scratching behavior induced by bombesin (0.2 nmol/10 μl, i.t.) in mice injected with AAV-hM4Di-mCitrine or AAV-EGFP in the PBN (*n* = 7 for each group). (**B-D**) Effect of pharmacogenetic inhibition of PBN on the nociceptive response tested by von Frey (**B**), Hargreaves (**C**), and tail-flick tests (**D**) measured 30 min after CNO (1 mg/kg, i.p.) or vehicle injection (*n* = 6 for each group). (**E**, **F**) Example traces of open field test for AAV-EGFP (**E**) and AAV-hM4Di-mCitrine group (**F**). (**G**, **H**) Pharmacogenetic inhibition of PBN didn't affect locomotor activity tested by open field test (*n* = 8 for each group). Time in center (**G**) and total distance (**H**) showed no significant difference between AAV-EGFP and AAV-hM4Di-mCitrine group (*n* = 8 for each group). (**I**) Pharmacogenetic inhibition of PBN didn't affect motor function tested by rotarod test (*n* = 4 for each group). Error bars represent SEM. *$P < 0.05$, unpaired t-test.
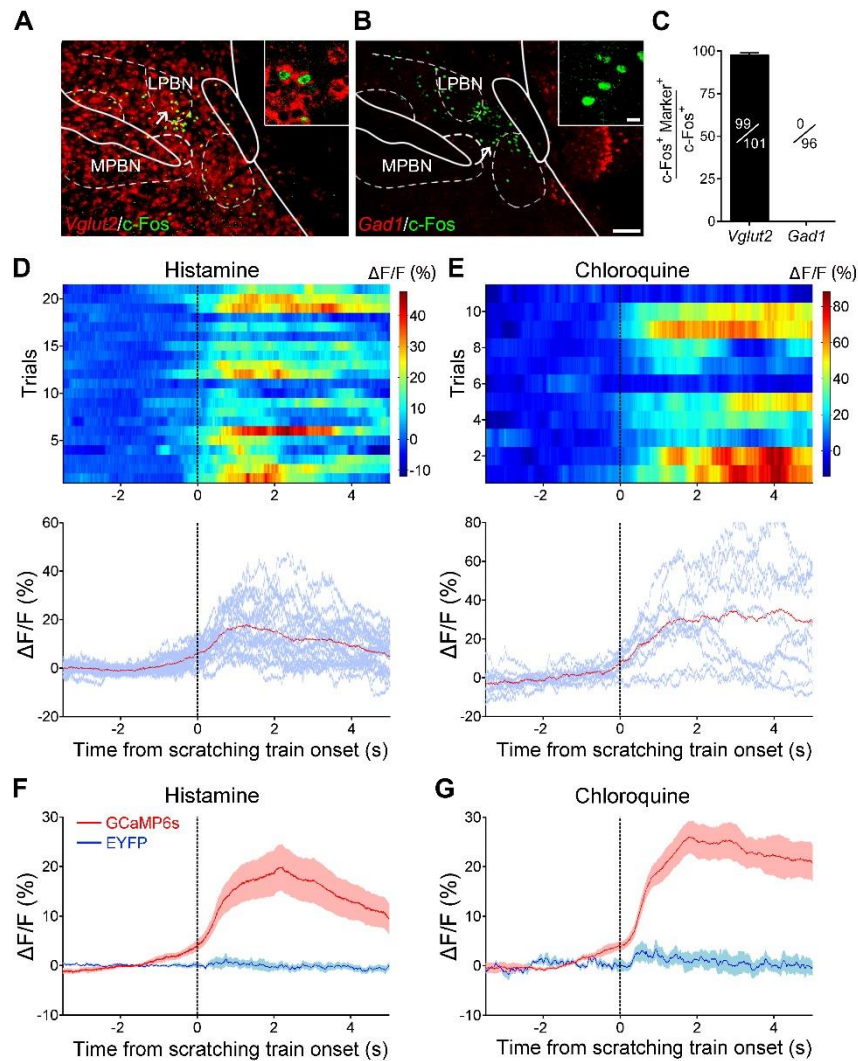
Fig. S10. Activity of PBN glutamatergic neurons increased during itch-induced scratching behavior.

(**A**) Double staining of c-Fos and *Vglut2* with immunostaining and fluorescence *in situ* hybridization respectively in the PBN of mice received intradermal injection of histamine (500 μg/50 μl). Red, *Vglut2* fluorescence *in situ* hybridization; green, c-Fos immunostaining. (**B**) Double staining of c-Fos and *Gad1* with immunostaining and fluorescence *in situ* hybridization respectively in the PBN of mice received intradermal injection of histamine (500 μg/50 μl). Red, *Gad1* fluorescence *in situ* hybridization; green, c-Fos immunostaining. Scale bars: B, 100 μm, inset in B, 10 μm. (**C**) Percentage of c-Fos⁺ cells that express *Vglut2* or *Gad1* (*n* = 3 mice). Error bars represent SEM. (**D**) A representative experiment showing the Ca²⁺ transients associated with scratching behavior induced by histamine in a *Vglut2-Cre* mouse injected with AAV-DIO-GCaMP6s in the PBN. Top, heat map of fluorescence changes in all scratching trains aligned to the scratching train onset. Bottom, raw data of the same mouse were shown in blue, and the red trace represents the average of all traces for Ca²⁺ transients. (**E**) A representative experiment showing the Ca²⁺ transients associated with scratching behavior induced by chloroquine in a *Vglut2-Cre* mouse

25

injected with AAV-DIO-GCaMP6s in the PBN. Top, heat map of fluorescence changes in all scratching trains aligned to the scratching train onset. Bottom, raw data of the same mouse were shown in blue, and the red trace represents the average of all traces for Ca^{2+} transients. (**F**) Average fluorescence change of PBN glutamatergic neurons of *Vglut2-Cre* mice injected with AAV-DIO-GCaMP6s ($n = 9$) 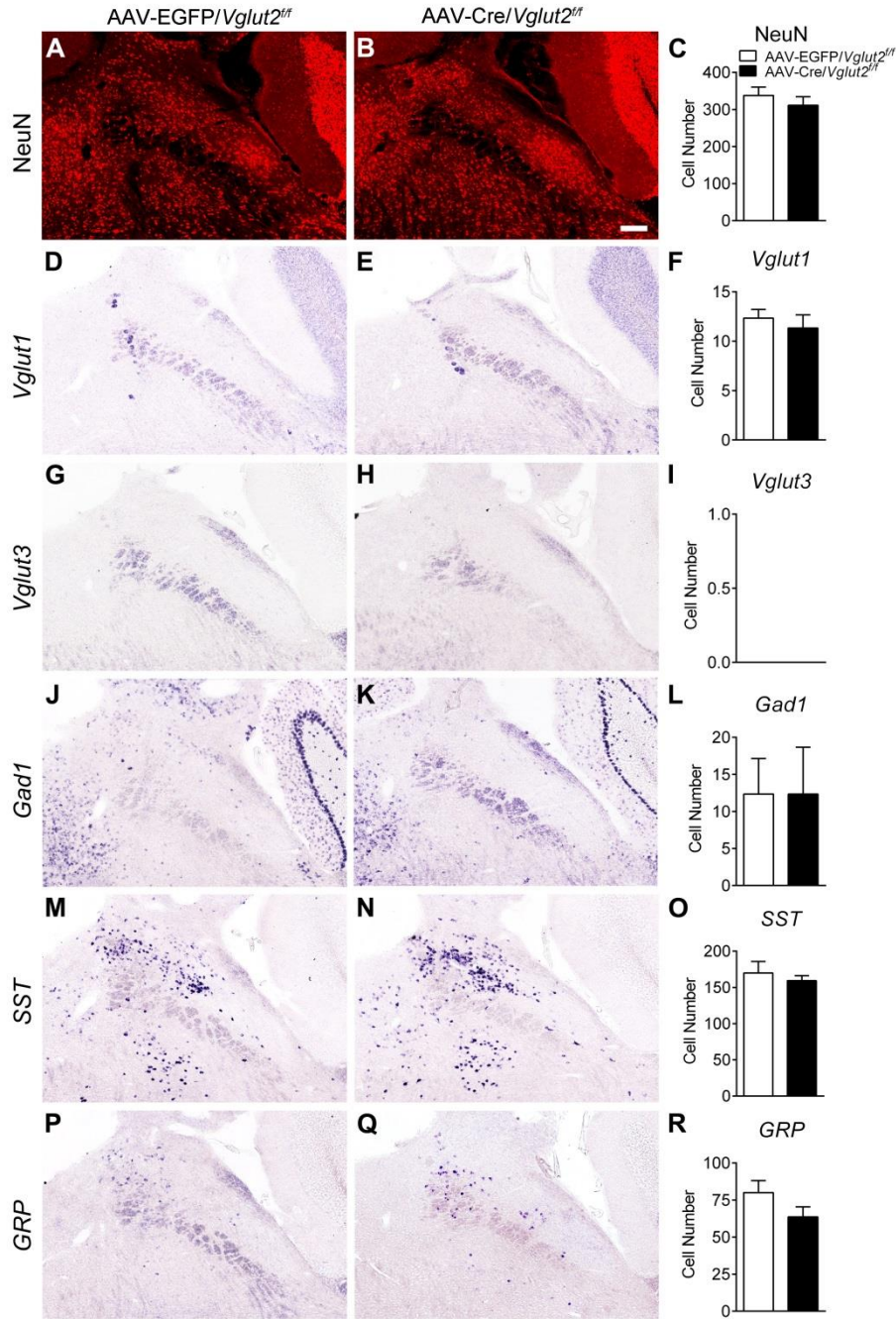or AAV-DIO-EYFP ($n = 6$) in the PBN in histamine model, shaded area indicates SEM. (**G**) Average fluorescence change of PBN glutamatergic neurons of *Vglut2-Cre* mice injected with AAV-DIO-GCaMP6s ($n = 7$) or AAV-DIO-EYFP ($n = 4$) in the PBN in chloroquine model, shaded area indicates SEM.

Fig. S11. Effect of genetic deletion of *Vglut2* on the expression of other molecular markers in the PBN.

(**A-C**) Knockout of *Vglut2* in the PBN didn't change the number of NeuN$^+$ cells (n = 4-6 mice). (**D-I**) Knockout of *Vglut2* in the PBN didn't cause compensative expression of other isoforms of vesicular glutamate transporter, including *Vglut1* (**D-F**) and *Vglut3* (**G-I**). (**J-L**) Expression of *Gad1*, an inhibitory neuron marker was not altered in the PBN after genetic deletion of *Vglut2*. (**M-O**) The number of somatostatin (*Sst*) positive neurons was comparable between AAV-Cre-EGFP/*Vglut2*$^{f/f}$ and AAV-EGFP/*Vglut2*$^{f/f}$ group. (**P-R**) The number of gastrin releasing peptide (*Grp*) positive neurons was comparable between

AAV-Cre-EGFP/*Vglut2$^{f/f}$* and AAV-EGFP/*Vglut2$^{f/f}$* group. $n = 3$ mice for each group. Scale bar: **B**, 150 μm. Error bars represent SEM.
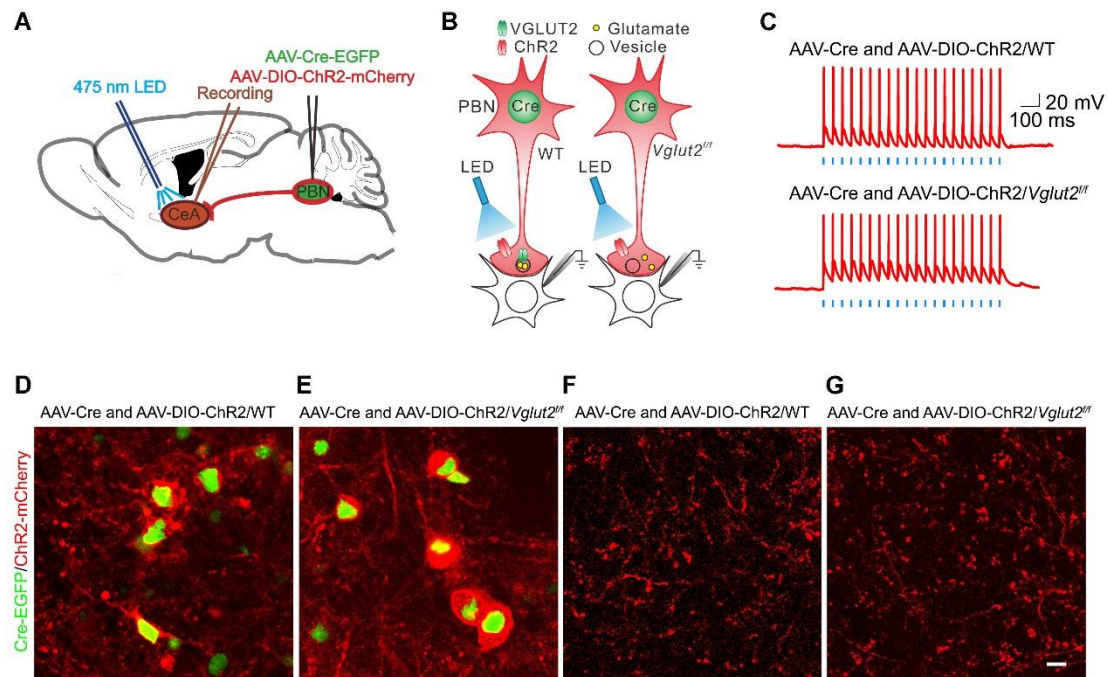
Fig. S12. Blockade of glutamatergic output by deletion of *Vglut2* in the PBN.

(**A**) Schematic illustrating injection of mixture of AAV-Cre-EGFP and AAV-DIO-ChR2-mCherry viruses into the PBN of *Vglut2^{f/f}* or wild-type mice, as well as patch clamp recording configuration in the amygdala. (**B**) Schematic depicting the strategy for testing the functional efficiency of deleting *Vglut2* in blocking glutamatergic output of the PBN. (**C**) Example traces showing that photostimulation (475 nm, 1 ms, 20 Hz) induced comparable action potentials in ChR2-mCherry^{+} neurons of the PBN of *Vglut2^{f/f}* and wild-type mice. (**D**, **E**) Example images showing the expression of AAV-Cre-EGFP and AAV-DIO-ChR2-mCherry in the PBN of *Vglut2^{f/f}* and wild-type mice after the virus injection. (**F**, **G**) Distribution of mCherry[+] fibers in the amygdala is comparable between *Vglut2^{f/f}* and wild-type mice one month after the virus injection. Similar results were obtained in another 2 mice. Scale bar: 10 μm.
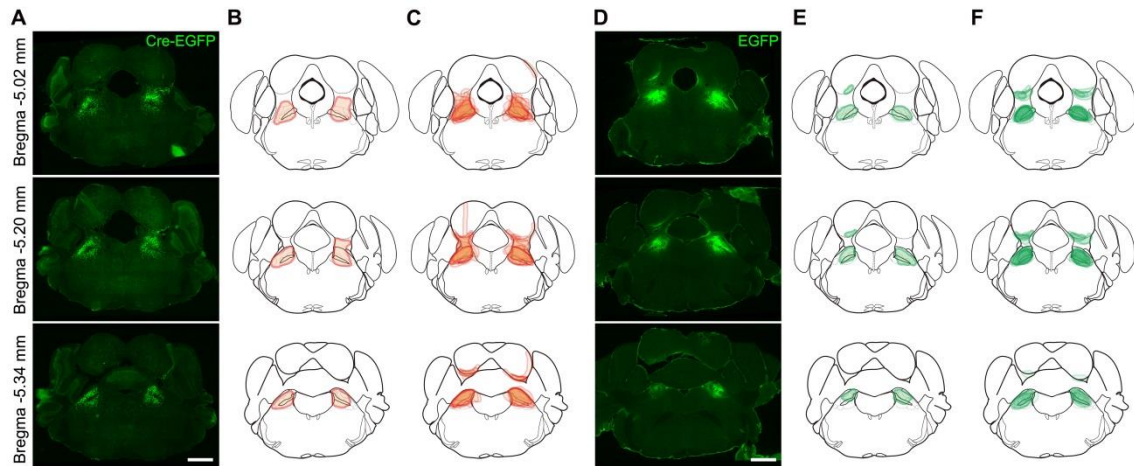
Fig. S13. Virus infection areas in the PBN of animals in AAV-Cre-EGFP and AAV-EGFP group.

(**A**) Representative images from a mouse injected with AAV-Cre-EGFP virus in the PBN. Scale bar, 1 mm. (**B**) Depiction of virus infection area according to the fluorescent images in **A**. (**C**) Superimp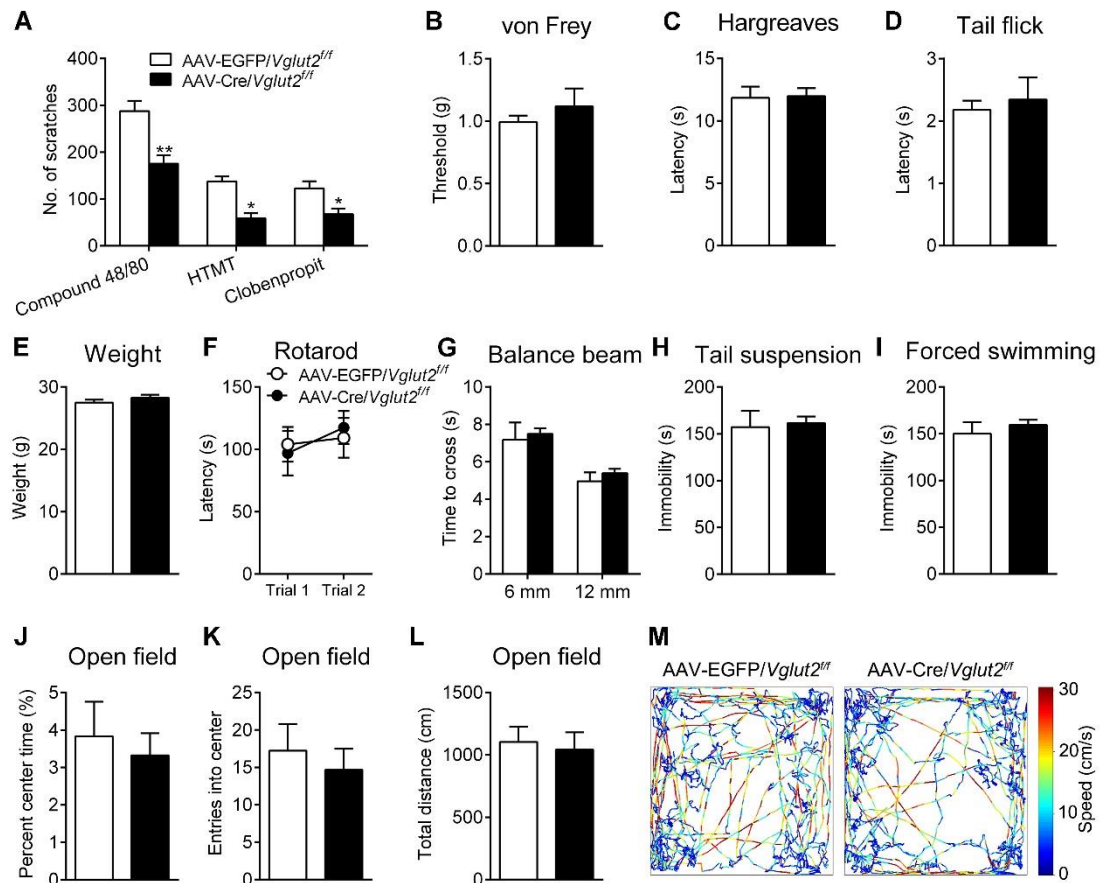osed depiction of virus infection areas for 6 mice in AAV-Cre-EGFP group. (**D**) Representative images from a mouse injected with AAV-EGFP virus in the PBN. Scale bar, 1 mm. (**E**) Depiction of virus infection areas according to the fluorescent images in **D**. (**F**) Superimposed depiction of virus infection areas for 6 mice in AAV-EGFP group.

Fig. S14. Effects of genetic deletion of *Vglut2* in the PBN on mouse behavior.

(**A**) Effects of genetic deletion of *Vglut2* in the PBN on scratching behavior induced by intradermal injection of compound 48/80 (100 μg/50 μl), HTMT (0.1 μmol/50 μl) or clobenpropit (0.1 μmol/50 μl), $n = 7$-12. (**B**-**D**) Effects of genetic deletion of *Vglut2* in the PBN on the nociceptive response tested by von Frey (**B**), Hargreaves (**C**) and tail-flick tests (**D**), $n = 10$-14. (**E**) Body weight of animals with genetic deletion of *Vglut2* in the PBN and the control group five weeks after viral injection ($n = 12$-16). (**F**, **G**) Motor function was comparable between the two groups as tested in rotarod (**F**) and balance beam (**G**) tests ($n = 9$ for each group). (**H**, **I**) The duration of immobility is comparable between two groups measured in tail-suspension (**H**) and forced swimming (**I**) tests ($n = 7$-9). (**J**-**L**) Deletion of *Vglut2* in the PBN didn't affect the activity measured with open field test ($n = 9$). (**M**) Example tracts of mice from the AAV-EGFP/*Vglut2^{f/f}* group (left panel) or the AAV-Cre-EGFP/*Vglut2^{f/f}* group (right panel) running in the open field test. Error bars represent SEM. *$P < 0.05$, **$P < 0.01$, unpaired t-test.

Movie S1. Recording of scratching behavior with two methods.

We used a magnetic induction method to record mice scratching behavior while videotaping the behavior with a high-speed camera (120 Hz). This video was slowed down by 10 times. Each up-down movement of the right hindpaw corresponds to a current peak in the recording trace.

References and Notes

1. A. L. Oaklander, S. P. Cohen, S. V. Raju, Intractable postherpetic itch and cutaneous deafferentation after facial shingles. *Pain* **96**, 9–12 (2002). [doi:10.1016/S0304-3959(01)00400-6](doi:10.1016/S0304-3959(01)00400-6) Medline

2. S. Bourane, B. Duan, S. C. Koch, A. Dalet, O. Britz, L. Garcia-Campmany, E. Kim, L. Cheng, A. Ghosh, Q. Ma, M. Goulding, Gate control of mechanical itch by a subpopulation of spinal cord interneurons. *Science* **350**, 550–554 (2015). doi:10.1126/science.aac8653 Medline

3. D. P. Roberson, S. Gudes, J. M. Sprague, H. A. W. Patoski, V. K. Robson, F. Blasl, B. Duan, S. B. Oh, B. P. Bean, Q. Ma, A. M. Binshtok, C. J. Woolf, Activity-dependent silencing reveals functionally distinct itch-generating sensory neurons. *Nat. Neurosci.* **16**, 910–918 (2013). [doi:10.1038/nn.3404](doi:10.1038/nn.3404) Medline

4. S. E. Ross, A. R. Mardinly, A. E. McCord, J. Zurawski, S. Cohen, C. Jung, L. Hu, S. I. Mok, A. Shah, E. M. Savner, C. Tolias, R. Corfas, S. Chen, P. Inquimbert, Y. Xu, R. R. McInnes, F. L. Rice, G. Corfas, Q. Ma, C. J. Woolf, M. E. Greenberg, Loss of inhibitory interneurons in the dorsal spinal cord and elevated itch in Bhlhb5 mutant mice. *Neuron* **65**, 886–898 (2010). doi:10.1016/j.neuron.2010.02.025 Medline

5. Y. G. Sun, Z. F. Chen, A gastrin-releasing peptide receptor mediates the itch sensation in the spinal cord. *Nature* **448**, 700–703 (2007). doi:10.1038/nature06029 Medline

6. Q. Liu, Z. Tang, L. Surdenikova, S. Kim, K. N. Patel, A. Kim, F. Ru, Y. Guan, H.-J. Weng, Y. Geng, B. J. Undem, M. Kollarik, Z.-F. Chen, D. J. Anderson, X. Dong, Sensory neuron-specific GPCR Mrgprs are itch receptors mediating chloroquine-induced pruritus. *Cell* **139**, 1353–1365 (2009). doi:10.1016/j.cell.2009.11.034 Medline

7. R. H. LaMotte, X. Dong, M. Ringkamp, Sensory neurons and circuits mediating itch. *Nat. Rev. Neurosci.* **15**, 19–31 (2014). [doi:10.1038/nrn3641](doi:10.1038/nrn3641) Medline

8. H. Mochizuki, R. Kakigi, Central mechanisms of itch. *Clin. Neurophysiol.* **126**, 1650–1660 (2015). doi:10.1016/j.clinph.2014.11.019 Medline

9. L. Herde, C. Forster, M. Strupf, H. O. Handwerker, Itch induced by a novel method leads to limbic deactivations a functional MRI study. *J. Neurophysiol.* **98**, 2347–2356 (2007). [doi:10.1152/jn.00475.2007](doi:10.1152/jn.00475.2007) Medline

10. G. Yosipovitch, Y. Ishiuji, T. S. Patel, M. I. Hicks, Y. Oshiro, R. A. Kraft, E. Winnicki, R. C. Coghill, The brain processing of scratching. *J. Invest. Dermatol.* **128**, 1806–1811 (2008). [doi:10.1038/jid.2008.3](doi:10.1038/jid.2008.3) Medline

11. D. Andrew, A. D. Craig, Spinothalamic lamina I neurons selectively sensitive to histamine: A central neural pathway for itch. *Nat. Neurosci.* **4**, 72–77 (2001). [doi:10.1038/82924](doi:10.1038/82924) Medline

12. S. Davidson, X. Zhang, C. H. Yoon, S. G. Khasabov, D. A. Simone, G. J. Giesler Jr., The itch-producing agents histamine and cowhage activate separate populations of primate spinothalamic tract neurons. *J. Neurosci.* **27**, 10007–10014 (2007). doi:10.1523/JNEUROSCI.2862-07.2007 Medline

13. S. Han, M. T. Soleiman, M. E. Soden, L. S. Zweifel, R. D. Palmiter, Elucidating an affective pain circuit that creates a threat memory. *Cell* **162**, 363–374 (2015). doi:10.1016/j.cell.2015.05.057 Medline

14. Z. Q. Zhao, L. Wan, X.-Y. Liu, F.-Q. Huo, H. Li, D. M. Barry, S. Krieger, S. Kim, Z.-C. Liu, J. Xu, B. E. Rogers, Y.-Q. Li, Z.-F. Chen, Cross-inhibition of NMBR and GRPR signaling maintains normal histaminergic itch transmission. *J. Neurosci.* **34**, 12402–12414 (2014). doi:10.1523/JNEUROSCI.1709-14.2014 Medline

15. M. S. Weiss, J. D. Victor, P. M. Di Lorenzo, Taste coding in the parabrachial nucleus of the pons in awake, freely licking rats and comparison with the nucleus of the solitary tract. *J. Neurophysiol.* **111**, 1655–1670 (2014). doi:10.1152/jn.00643.2013 Medline

16. N. A. Jansen, G. J. Giesler Jr., Response characteristics of pruriceptive and nociceptive trigeminoparabrachial tract neurons in the rat. *J. Neurophysiol.* **113**, 58–70 (2015). doi:10.1152/jn.00596.2014 Medline

17. D. Cameron, E. Polgár, M. Gutierrez-Mecinas, M. Gomez-Lima, M. Watanabe, A. J. Todd, The organisation of spinoparabrachial neurons in the mouse. *Pain* **156**, 2061–2071 (2015). doi:10.1097/j.pain.0000000000000270 Medline

18. T. Akiyama, T. Nguyen, E. Curtis, K. Nishida, J. Devireddy, J. Delahanty, M. I. Carstens, E. Carstens, A central role for spinal dorsal horn neurons that express neurokinin-1 receptors in chronic itch. *Pain* **156**, 1240–1246 (2015). doi:10.1097/j.pain.0000000000000172 Medline

19. Y. G. Sun, Z.-Q. Zhao, X.-L. Meng, J. Yin, X.-Y. Liu, Z.-F. Chen, Cellular basis of itch sensation. *Science* **325**, 1531–1534 (2009). doi:10.1126/science.1174868 Medline

20. D. M. Bautista, S. R. Wilson, M. A. Hoon, Why we scratch an itch: The molecules, cells and circuits of itch. *Nat. Neurosci.* **17**, 175–182 (2014). doi:10.1038/nn.3619 Medline

21. S. K. Mishra, M. A. Hoon, The cells and circuitry for itch responses in mice. *Science* **340**, 968–971 (2013). doi:10.1126/science.1233765 Medline

22. X. Wang, J. Zhang, D. Eberhart, R. Urban, K. Meda, C. Solorzano, H. Yamanaka, D. Rice, A. I. Basbaum, Excitatory superficial dorsal horn interneurons are functionally heterogeneous and required for the full behavioral expression of pain and itch. *Neuron* **78**, 312–324 (2013). doi:10.1016/j.neuron.2013.03.001 Medline

23. L. A. Gunaydin, L. Grosenick, J. C. Finkelstein, I. V. Kauvar, L. E. Fenno, A. Adhikari, S. Lammel, J. J. Mirzabekov, R. D. Airan, K. A. Zalocusky, K. M. Tye, P. Anikeeva, R. C. Malenka, K. Deisseroth, Natural neural projection dynamics underlying social behavior. *Cell* **157**, 1535–1551 (2014). doi:10.1016/j.cell.2014.05.017 Medline

24. B. N. Armbruster, X. Li, M. H. Pausch, S. Herlitze, B. L. Roth, Evolving the lock to fit the key to create a family of G protein-coupled receptors potently activated by an inert ligand. *Proc. Natl. Acad. Sci. U.S.A.* **104**, 5163–5168 (2007). doi:10.1073/pnas.0700293104 Medline

25. Q. Tong, C. Ye, R. J. McCrimmon, H. Dhillon, B. Choi, M. D. Kramer, J. Yu, Z. Yang, L. M. Christiansen, C. E. Lee, C. S. Choi, J. M. Zigman, G. I. Shulman, R. S. Sherwin, J. K. Elmquist, B. B. Lowell, Synaptic glutamate release by ventromedial hypothalamic

neurons is part of the neurocircuitry that prevents hypoglycemia. *Cell Metab.* **5**, 383–393 (2007). doi:10.1016/j.cmet.2007.04.001 Medline

26. O. R. Hyndman, J. Wolkin, Anterior cordotomy: Further observations on the physiologic results and optimum manner of performance. *Arch. Neurol. Psychiatry* **50**, 129–148 (1943). doi:10.1001/archneurpsyc.1943.02290200029002

27. S. Davidson, G. J. Giesler, The multiple pathways for itch and their interactions with pain. *Trends Neurosci.* **33**, 550–558 (2010). doi:10.1016/j.tins.2010.09.002 Medline

28. S. F. Giszter, J. McIntyre, E. Bizzi, Kinematic strategies and sensorimotor transformations in the wiping movements of frogs. *J. Neurophysiol.* **62**, 750–767 (1989). Medline

29. M. Wiberg, J. Westman, A. Blomqvist, Somatosensory projection to the mesencephalon: An anatomical study in the monkey. *J. Comp. Neurol.* **264**, 92–117 (1987). doi:10.1002/cne.902640108 Medline

30. A. D. Craig, Distribution of brainstem projections from spinal lamina I neurons in the cat and the monkey. *J. Comp. Neurol.* **361**, 225–248 (1995). doi:10.1002/cne.903610204 Medline

31. N. Inagaki, K. Igeta, J. F. Kim, M. Nagao, N. Shiraishi, N. Nakamura, H. Nagai, Involvement of unique mechanisms in the induction of scratching behavior in BALB/c mice by compound 48/80. *Eur. J. Pharmacol.* **448**, 175–183 (2002). doi:10.1016/S0014-2999(02)01933-7 Medline

32. L. Han, C. Ma, Q. Liu, H.-J. Weng, Y. Cui, Z. Tang, Y. Kim, H. Nie, L. Qu, K. N. Patel, Z. Li, B. McNeil, S. He, Y. Guan, B. Xiao, R. H. Lamotte, X. Dong, A subpopulation of nociceptors specifically linked to itch. *Nat. Neurosci.* **16**, 174–182 (2013). doi:10.1038/nn.3289 Medline

33. X. J. Liu, Y. Zhang, T. Liu, Z.-Z. Xu, C.-K. Park, T. Berta, D. Jiang, R.-R. Ji, Nociceptive neurons regulate innate and adaptive immunity and neuropathic pain through MyD88 adapter. *Cell Res.* **24**, 1374–1377 (2014). doi:10.1038/cr.2014.106 Medline

34. S. R. Chaplan, F. W. Bach, J. W. Pogrel, J. M. Chung, T. L. Yaksh, Quantitative assessment of tactile allodynia in the rat paw. *J. Neurosci. Methods* **53**, 55–63 (1994). doi:10.1016/0165-0270(94)90144-9 Medline

35. J. C. Patel, E. Rossignol, M. E. Rice, R. P. Machold, Opposing regulation of dopaminergic activity and exploratory motor behavior by forebrain and brainstem cholinergic circuits. *Nat. Commun.* **3**, 1172 (2012). doi:10.1038/ncomms2144 Medline

36. T. N. Luong, H. J. Carlisle, A. Southwell, P. H. Patterson, Assessment of motor balance and coordination in mice using the balance beam. *J. Vis. Exp.* **49**, e2376 (2011). Medline

37. I. Lucki, A. Dalvi, A. J. Mayorga, Sensitivity to the effects of pharmacologically selective antidepressants in different strains of mice. *Psychopharmacology (Berl.)* **155**, 315–322 (2001). doi:10.1007/s002130100694 Medline

38. Z. Q. Zhao, Y.-J. Gao, Y.-G. Sun, C.-S. Zhao, R. W. Gereau 4th, Z.-F. Chen, Central serotonergic neurons are differentially required for opioid analgesia but not for morphine tolerance or morphine reward. *Proc. Natl. Acad. Sci. U.S.A.* **104**, 14519–14524 (2007). doi:10.1073/pnas.0705740104 Medline

39. Y. G. Sun, C. S. Wu, H. C. Lu, M. Beierlein, Target-dependent control of synaptic inhibition by endocannabinoids in the thalamus. *J. Neurosci.* **31**, 9222–9230 (2011). doi:10.1523/JNEUROSCI.0531-11.2011 Medline

40. Y. G. Sun, V. Rupprecht, L. Zhou, R. Dasgupta, F. Seibt, M. Beierlein, mGluR1 and mGluR5 synergistically control cholinergic synaptic transmission in the thalamic reticular nucleus. *J. Neurosci.* **36**, 7886–7896 (2016). doi:10.1523/JNEUROSCI.0409-16.2016 Medline

41. C. Luo, V. Gangadharan, K. K. Bali, R.-G. Xie, N. Agarwal, M. Kurejova, A. Tappe-Theodor, I. Tegeder, S. Feil, G. Lewin, E. Polgar, A. J. Todd, J. Schlossmann, F. Hofmann, D.-L. Liu, S.-J. Hu, R. Feil, T. Kuner, R. Kuner, Presynaptically localized cyclic GMP-dependent protein kinase 1 is a key determinant of spinal synaptic potentiation and pain hypersensitivity. *PLOS Biol.* **10**, e1001283 (2012). doi:10.1371/journal.pbio.1001283 Medline

42. M. Goard, Y. Dan, Basal forebrain activation enhances cortical coding of natural scenes. *Nat. Neurosci.* **12**, 1444–1449 (2009). doi:10.1038/nn.2402 Medline